Biosensors and Bioelectronics 70 (2015) 226–231

Contents lists available at ScienceDirect

Biosensors and Bioelectronics

journal homepage: www.elsevier.com/locate/bios

Rapid and sensitive detection of multiple microRNAs in cell lysate by low-fouling surface plasmon resonance biosensor

Hana Vaisocherová [a], Hana Šípová [a], Ivana Víšová [a], Markéta Bocková [a], Tomáš Špringer [a], Maria Laura Ermini [a], Xue Song [a], Zdeněk Krejčík [b], Leona Chrastinová [b], Ondřej Pastva [b], Kristýna Pimková [a,b], Michaela Dostálová Merkerová [b], Jan E. Dyr [b], Jiří Homola [a,*]

[a] Institute of Photonics and Electronics, Academy of Sciences of the Czech Republic, Chaberská 57, 18251 Prague, Czech Republic
[b] Institute of Hematology and Blood Transfusion, U Nemocnice 1, 12820 Prague, Czech Republic

ARTICLE INFO

Article history:
Received 5 December 2014
Received in revised form
5 March 2015
Accepted 16 March 2015
Available online 17 March 2015

Keywords:
Low-fouling surface chemistry
DNA array
microRNA
Polymer brushes
Surface plasmon resonance imaging
Erythrocyte lysate

ABSTRACT

We report an ultra-low fouling surface plasmon resonance imaging (SPRi) biosensor for the rapid simultaneous detection of multiple miRNAs in erythrocyte lysate (EL) at subpicomolar levels without need of RNA extraction. The SPRi chips were coated with ultra-low fouling functionalizable poly(carboxybetaine acrylamide) (pCBAA) brushes having optimized thicknesses and directly functionalized with amino-modified oligonucleotide probes. We have characterized the effect of the brush thickness on the probe loading capacity: a loading capacity of $\sim 9.8 \times 10^{12}$ probes/cm^2 was achieved for pCBAA having a thickness of ~40 nm. The probe-functionalized sensor also exhibited a high resistance to fouling from ~90% EL samples (< 2 ng/cm^2). A two-step detection assay was employed for multiplexed miRNA detection in EL. Specifically, the assay consisted of (i) a sandwich-type hybridization of the probe-functionalized pCBAA with target miRNA in EL (bound to biotinylated oligonucleotides) and (ii) the capture of streptavidin-functionalized gold nanoparticles to the aforementioned biotinylated probes. We have demonstrated that this approach enables the detection of miRNAs in EL at concentrations as low as 0.5 pM. Finally, we have confirmed the detection of four endogenous miRNAs representing a set of potential miRNA biomarkers of myelodysplastic syndrome (MDS) in clinical EL samples (miR-16, miR-181, miR-34a, and miR-125b). The results revealed significantly higher levels of miR-16 in all the clinical EL samples compared to the other measured miRNAs.

1. Introduction

Mature microribonucleic acids (miRNAs) are ~19–24 nucleotide long noncoding RNAs that regulate gene expression in living cells by mediating targeted hydrolysis and translation inhibition of messenger RNAs (He and Hannon, 2004). The miRNAs present in erythrocyte lysate (EL) play an important role in erythropoiesis and final mRNA degradation (Farh et al., 2005; Felli et al., 2005; Georgantas et al., 2007). Although the complex mechanism of miRNA-induced regulation of gene expression is still not fully understood, numerous intracellular and circulating miRNAs have been linked to disease outcomes and prognosis (Iorio et al., 2005; Lu et al., 2005). Moreover, there has been increasing evidence over the last five years suggesting that changes in miRNA levels in bodily fluids and tissues are closely associated with the pathogenesis of most human malignancies, including myelodysplastic syndrome (MDS) or cardiovascular disease (Erdogan et al., 2011; Ikeda et al., 2007; Iorio et al., 2005; Lu et al., 2005; Wang et al., 2009).

Accordingly, miRNAs represent an attractive target as potential disease biomarkers. Although methods for the detection of nucleic acids are well established, there remain great challenges for the accurate and reliable quantification of miRNAs in bodily fluids. These challenges include miRNAs having short sequences, low concentrations of target miRNAs in analyzed samples, and interferences from complex sample matrices (Engels and Hutvagner, 2006; Gao et al., 2014).

Conventional methods for the detection of miRNA include quantitative reverse-transcription real-time polymerase chain reaction (RT-qPCR), microarrays, and northern blotting (Benes and Castoldi, 2010; Lagos-Quintana et al., 2002; Thomson et al., 2004; Wark et al., 2008). Unlike semi-quantitative northern blotting-based approaches (Kuchar et al., 2014; Valoczi et al., 2004), RT-qPCR can cover a broad dynamic range of miRNA concentrations with a relatively high sensitivity. Unfortunately, this method is rather time consuming and requires expensive and complex

* Corresponding author.
E-mail address: homola@ufe.cz (J. Homola).

http://dx.doi.org/10.1016/j.bios.2015.03.038
0956-5663/

equipment. Furthermore, because highly purified samples are required, the extraction of miRNA from complex biological samples is necessary. Due to the lack of standardized protocols for miRNA extraction, this extraction step may lead to increases in variability and decreases in accuracy (McAlexander et al., 2013; Turchinovich et al., 2012). Microarrays enable parallelized detection of multiple miRNAs (Thomson et al., 2004); however, the complexity of miRNA labeling, insufficient sensitivity, long hybridization times, or challenges for standardization limit the routine use of microarrays in centralized laboratories (Liu et al., 2004).

Several biosensing methods have been proposed as alternative methods to detect miRNAs. These biosensors include those based on (photo)electrochemistry (Dong et al., 2012; Gao et al., 2013; Ge et al., 2014; Kilic et al., 2012; Li et al., 2014; Yin et al., 2014, 2012; Zhu et al., 2014), electrochemiluminiscence (Cheng et al., 2014; Liu et al., 2014), fluorescence quenching (Dong et al., 2014; Guo et al. ,2014; Ryoo et al., 2013), and surface plasmon resonance (SPR) (Sipova et al., 2010; Zhang et al., 2013). The majority of these studies involve the detection of miRNA either in buffer, diluted complex bodily fluids, or in aqueous solutions of reconstituted RNA extracts (Dong et al., 2014; Wen et al., 2013; Yin et al., 2014). Only a few of these studies involve the detection of miRNA directly in a complex biological sample (without the sample pre-treatment miRNA extraction step). For instance, Yin et al. reported the ultrasensitive detection of miR-21 in diluted human serum (LOD of 100aM for miR-21 detection in a buffer) using an electrochemical biosensor; however, this technique had rather long detection time (>4 h) (Yin et al., 2012). In addition, Ryoo et al. recently reported a fluorescence label-based optical sensor that utilized peptide nucleic acid (PNA) and nano-sized graphene oxide. The sensor was capable of multiplexed detection of miRNAs at picomolar levels in living cells (Ryoo et al., 2013).

In this work, we present a label-free optical biosensor based on surface plasmon resonance imaging (SPRi) that allows for rapid (<1 h) and multiplexed detection of miRNAs in EL samples without the need for miRNA extraction or pre-amplification. The sensor employs carboxy-functional ultra-low fouling polymer brushes with amino-modified probes for a two-step assay, which utilizes sandwich-type hybridization in EL in addition to signal amplification by streptavidin-functionalized gold nanoparticles (S-AuNPs). We explore the effects of the brush thickness on the surface loading capacity and the resistance to fouling from EL. We targeted four miRNAs (miR-16, miR-181, miR-34a, and miR-125b) that represent potential myelodysplastic syndrome (MDS) biomarkers (McAlexander et al., 2013; Peng and Gao, 2011; Rhyasen and Starczynowski, 2012). After establishing a set of calibration curves for these miRNAs spiked in EL, we screened three clinical EL samples for the levels of native endogenous miRNAs.

2. Materials and methods

2.1. Reagents and erythrocyte lysate samples

The list of reagents used in this work and procedure of preparation of erythrocyte lysate samples is provided in the Supplementary material. Spherical gold nanoparticles (AuNPs) with a diameter of 35 nm were prepared by the reduction of $HAuCl_4$ with sodium citrate (Bastus et al., 2011). Bare AuNPs were modified with carboxyl-terminated alkanethiols and then streptavidin was covalently bound to the surface of AuNPs by amine coupling chemistry (see Supplementary material).

2.2. SPR sensors

Two SPR systems developed at the Institute of Photonics and Electronics (Prague, Czech Republic) were used in this study. A high-resolution SPR imaging (SPRi) system with polarization contrast and internal referencing (Piliarik et al., 2010) combined with dispersionless microfluidics (Springer et al., 2010) was used in the detection experiments. This system enables the simultaneous analysis of biomolecular interactions in 30 individual flow-through sensing spots by using two separate flow-cells with perpendicularly oriented flow chambers. The first (six-channel) flow-cell was used for surface functionalization, while the second (with six perpendicularly oriented channels) was used for the detection (see also Supplementary material). A four-channel spectroscopic SPR sensor (Homola et al., 2002; Vaisocherova et al., 2014) was used for the optimization of surface functionalization, fouling studies, and assay control experiments. Both SPR sensors were equipped with a temperature controller, enabling SPR measurements in a temperature interval of 5–40 °C with a baseline stability of 0.01 °C. In order to compensate for the effect of decreasing SPR sensitivity with increasing layer thickness (Homola, 2008), the SPR sensor response obtained from both sensors was calibrated using previously described procedures (Piliarik et al., 2010; Vaisocherova et al., 2014). A typical value of the correction factor for bare polymer brush thickness was 1.29 for a 30 nm thick pCBAA (RI = 1.401 RIU at 750 nm for wet surface (Vaisocherova et al., 2014)). For the SPR sensors used in this study and a resonant wavelength of about 750 nm, a 1 mRIU SPRi sensor response corresponds to a $\sim$5.9 nm response of the spectroscopic SPR sensor (Piliarik et al., 2010). In terms of surface coverage, a SPRi sensor response of 1 mRIU corresponds to a change in the surface coverage of $\sim$100 ng/cm^2 (Homola, 2006; Vaisocherova et al., 2007).

2.3. SPR sensor measurements

The poly(carboxybetaine acrylamide) (pCBAA) coatings were prepared by atom transfer radical polymerization (ATRP) according to a previously described procedure (Vaisocherova et al., 2008). These procedures were carried out under optimized conditions in order to obtain coatings with a wet thickness in the range of 13–45 nm (Supplementary material). The thickness of wet brushes was measured by means of the spectroscopic SPR sensor via a previously described procedure (Vaisocherova et al., 2014).

The pCBAA surface functionalization was performed using a flow-through regime without extra spotting. The procedure consisted of three steps: (1) activation of the functional carboxyl groups by the NHS/EDC method adjusted to the physical–chemical properties of pCBAA (Vaisocherova et al., 2014), (2) covalent attachment of amino-modified oligonucleotide probes ($probe_1$ in Fig. 2), and (3) deactivation of any residual reactive groups. The optimized procedure for surface functionalization is provided in Supplementary material.

In the spiked miRNA detection experiments, the sample with miRNA was mixed with biotin-terminated probes ($probe_2$) having a complementary base sequence to the target miRNAs and flowed along the $probe_1$-functionalized pCBAA surface at 15 °C for 10 min (step I. in Fig. 2). This step resulted in the formation of stable miRNA*$probe_1$–$probe_2$ complexes on the pCBAA-coated sensor surface. In the second step of the assay, the sensor response to miRNA was enhanced with S-AuNPs. The S-AuNPs were flowed along the surface for 25 min at 15 °C and bound to $probe_2$ via the streptavidin–biotin interaction (step II. in Fig. 2).

In order to obtain the calibration curves, we carried out the detection of four miRNA spiked samples (miR-16, miR-34a, miR-181, and miR-125b) in EL or PBS at target concentrations of 0.1 pM, 0.5 pM, 1 pM, 100 pM, and 500 pM. Specifically, the undiluted EL sample taken from a healthy individual was spiked with aliquots of EDTA (5 mM), NaCl (150 mM), the biotin-terminated probes to

respective targets (probe$_2$, BdmiRNA, 0.5 μM), and miRNA targets in a concentration range of 0.1–500 pM. Samples were then heated to 50 °C and cooled down slowly to room temperature while gently mixing, after which SDS (0.5%) was added to each EL sample. It should be noted that after addition of all the reagents, the original solute concentration of each EL sample was not lower than 87% of the original value. At least two different miRNAs were detected simultaneously in a single sample using a single chip (Fig. S-3 in Supplementary material). These samples were flowed along surfaces functionalized with the corresponding probe$_1$ at 15 °C for 10 min, followed by the injection of S-AuNPs with OD 0.1 in PBS with BSA (200 μg/ml) for 25 min at 15 °C. An EL sample without miRNAs or BdmiRNAs (blank sample) was injected in a single channel to check the levels of non-specific S-AuNP binding (reference channel). To help control the surface homogeneity and deactivation after the activation/deactivation surface treatment, one additional control spot in each detection channel without immobilized probes within the same surface was identified using the SPRi software (see also Fig. S-3 in Supplementary material). The signals from the reference channels were subtracted from detection channels to compensate for potential flow disturbance, temperature fluctuations, sample composition variations, or non-specific binding. The change in sensor response to S-AuNPs binding was determined for each sample from the start (0 min) to end time (35 min after washing with PBS). The linear range of sensor detection was determined for each miRNA. The potential *y*-axis offsets corresponding to the presence of native endogenous miRNA in analyzed samples were subtracted. The limit of detection (LOD) was calculated based on the measurement of three blank EL samples by using "blank + 3 × SD" approach.

The effect of brush thickness on fouling from EL obtained from a healthy individual was measured at 25 °C for 15 min by flowing the EL sample over the NdmiR-16-functionalized pCBAA surfaces (with wet thickness of 20–40 nm, probe surface coverages were kept constant ($\sim 5.0 \times 10^{12}$ probe/cm^2). The fouling characteristics were determined after washing the surface with PBS buffer for 10 min.

Screening of clinical EL samples, i.e., a sample obtained from a healthy individual (Normal-1) and two samples from patients diagnosed with MDS (MDS-1, MDS-2)) was carried out using the SPRi instrument and the procedure described above (except for an injection of any samples spiked with miRNAs). The sensor response to S-AuNPs was converted to a concentration scale using previously determined sensor calibration curves. Validation of the method was performed using a reverse measurement of miR-16 in a control sample of a miRNA extracted from EL (MDS-3).

3. Results

3.1. Functionalization of SPR chips with pCBAA and amino-modified probes

The pCBAA surface functionalization was optimized in order to achieve a maximum loading capacity of immobilized probes while maintaining a surface resistance to fouling from EL, see Supplementary material.

In order to assess the effect of polymer brush thickness on the surface loading capacity, we prepared a series of pCBAA coatings with thicknesses in the range of 13–40 nm. The amino-modified probes for the detection of miR-16 were immobilized to the pCBAA layer using the optimized immobilization procedure. The results are shown in Fig. 1A. It can be seen that the loading capacity increased with increasing brush thickness, yielding a maximum capacity of $(9.8 \pm 0.6) \times 10^{12}$ probes/cm^2 for a pCBAA layer having a thickness of ~40 nm. The limited controllability of grafting

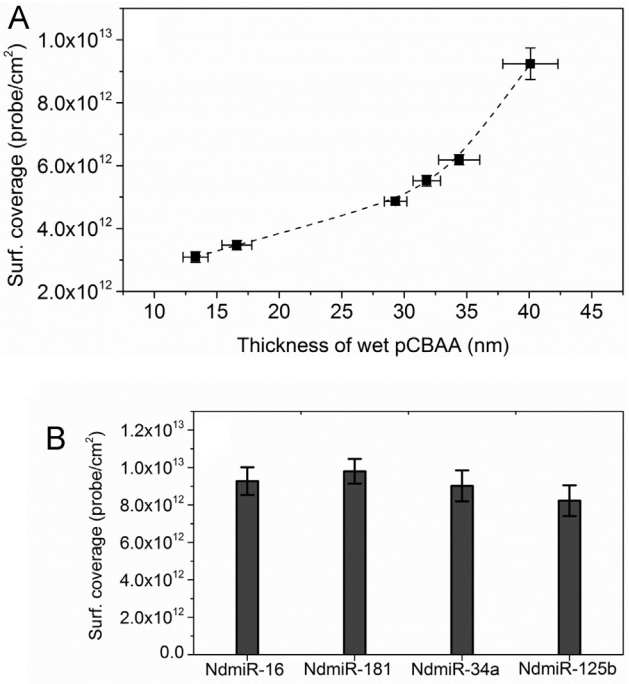

Fig. 1. (A) Effect of pCBAA wet thickness on probe immobilization levels measured by the SPR sensor. Data were averaged from at least three individual sensing channels functionalized with either NdmiR-16 or NdmiR-181. (B) Immobilization levels obtained for different amino-modified probes (NdmiR-16, NdmiR-181, NdmiR-34a, and NdmiR-125b) immobilized to pCBAA surfaces with a wet thickness of ~40 nm. Each data point was averaged from up to 18 sensing channels using 3 individual sensor chips.

pCBAA layers by ATRP (Rodriguez-Emmenegger et al., 2012) did not allow the preparation of reproducible pCBAA layers thicker than 40 nm; therefore, these were not included in this study. In this work, we assume that there exists a comparable pCBAA grafting density for brush thicknesses in the range of 19–40 nm (Vaisocherova et al., 2014).

The immobilization levels for all of the amino-modified probes used herein for pCBAA coatings with a maximum wet thickness of ~40 nm were comparable, ranging from 8.3×10^{12} probe/cm^2 to 9.8×10^{12} probe/cm^2 (Fig. 1B). A high chip-to-chip reproducibility (> 90%) of probe surface density on pCBAA (with a wet thickness of ~40 nm) was achieved for each probe. These probe immobilization levels are higher than those ($1–5 \times 10^{12}$ probe/cm^2) obtained using standard low-fouling oligo(ethylene glycol)-based mixed alkanethiolate self-assembled monolayers (OEG-based ATSAMs) functionalized with probes using the streptavidin–biotin interaction (Lahiri et al., 1999; Sipova and Homola, 2013; Vaisocherova et al., 2008). This finding is in agreement with the assumption that pCBAA brushes form 3D-like structures in solution, with good accessibility of reactive groups for probe coupling within the whole brush structure. Good accessibility of any reactive carboxyls within the hydrophilic pCBAA layer is facilitated by a high flexibility of the pCBAA brushes in aqueous solution (Vaisocherova et al., 2014).

3.2. Characterization of SPR biosensor for miRNA detection

A schematic representation of the two-step assay employed herein for the detection of miRNAs is shown in Fig. 2. The amino-modified probes (probe$_1$) were immobilized onto pCBAA-coated gold surfaces using the optimized procedure, where the pCBAA layer had a thickness of 35–42 nm. The SPR signal enhancement used in this miRNA assay is provided by S-AuNPs, whose adsorption within a close proximity to the gold planar surface generates a

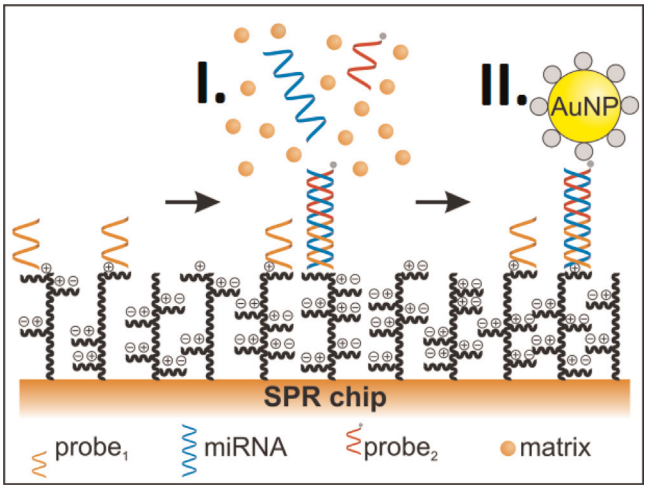

Fig. 2. Scheme of two-step assay employed for miRNA detection in erythrocyte lysate (EL) samples: First, the undiluted EL samples spiked with both biotinylated probes ($probe_2$) and miRNAs were flowed along the $probe_1$-functionalized pCBAA (step I.). Streptavidin-coated gold nanoparticles (S-AuNPs) were then injected to bind to $probe_2$ in order to enhance the sensor response to miRNA detection (step II.).

substantial increase in local refractive index. The used S-AuNPs provided an enhancement of approximately 800 × with respect to the sensor response for the detection of miRNA at a concentration of 2 nM, which is in good agreement with the amplification factor of S-AuNPs previously reported in literature (Springer et al., 2014).

In order to calibrate the sensor for the multiplexed detection of four miRNAs in EL, an EL sample (> 87%) was spiked with miRNAs of various concentrations in the range of 0.1–500 pM. Fig. 3A shows a representative reference-compensated sensor response to S-AuNPs binding to $probe_1$ covered pCBAA surface with miR-181∗$probe_2$ captured from the EL sample spiked with miR-181. Calibration curves for all the miRNAs are shown in Fig. 3B. We observed a minimum influence of the lysate matrix on the biosensor performance (Fig. S-5). The LODs determined from these calibration curves were 0.35 pM, 0.39 pM, 0.50 pM, and 0.95 pM for miR-16, miR-181, miR-34a, and miR-125b, respectively. The observed differences in the LOD may be attributed to differences in each nucleotide sequence that can affect the complex stability. This could be further improved by decreasing the sensor operating temperature to < 15 °C to enhance the oligonucleotide hybridization. Taking into account the sample volume that was analyzed (~300 µl), the LODs correspond to a total amount of miRNA in the range of hundreds of attomoles. Such LODs achieved are comparable to those recently obtained using the electrochemical and lateral-flow biosensors employed for single miRNA detection in miRNA buffered extracts and serum (Gao et al., 2013; Ren et al., 2013).

Control experiments were performed in order to characterize the sensor selectivity to miRNA sequences (see Supplementary material). No cross-reactivity between the oligonucleotides used in this study was observed under given experimental conditions.

In order to compare the SPR results with standard RT-qPCR method, total RNA was extracted from a EL sample and analyzed by both methods for the presence of native endogenous miR-16. The concentration of miR-16 determined by SPRi was 3.1 ± 1.0 pM and is in a very good agreement with the value obtained by RT-qPCR (4.0 ± 0.5 pM).

3.3. *Screening of clinical erythrocyte lysate samples for the levels of native miRNAs*

The SPRi biosensor was used for the detection of endogenous

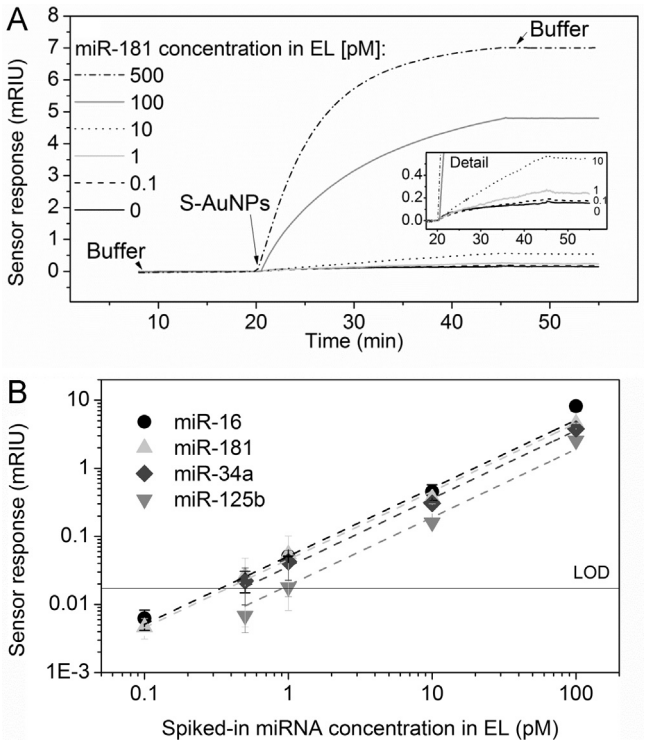

Fig. 3. (A) Representative SPRi data corresponding to S-AuNPs binding to miR-181∗NdmiR-181∗BdmiR-181 complexes immobilized on pCBAA. (B) Calibration curves for miR-16, miR-181, miR-34a, and miR-125b spiked into normal EL samples.

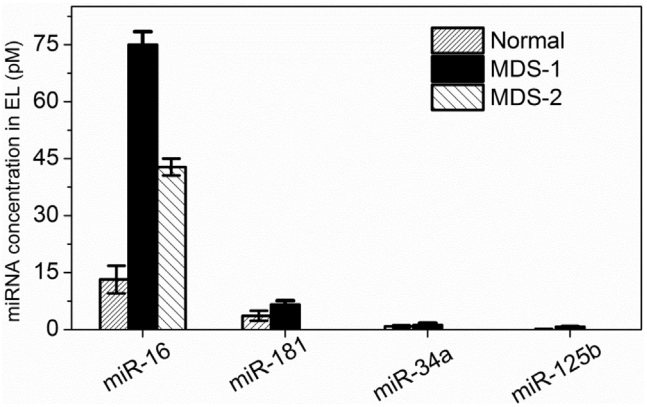

Fig. 4. Screening of clinical EL samples (Normal-1, MDS-1, and MDS-2) for miR-16, miR-181, miR-34a, and miR-125b using the SPRi biosensor. The results were averaged from at least 6 spots using 2 different SPR chips. The results from SPRi measurements were converted to concentrations using the previously established calibration curves.

levels of miR-16, miR-181, miR-34a, and miR-125b in EL samples (Normal-1, MDS-1, MDS-2), see Fig. 4 and Table S-3. The results from SPRi measurements were converted to concentrations using the previously established calibration curves, determined for each individual miRNA detection in EL sample. In all of the EL samples, miR-16 was found in significantly higher concentrations (at a concentration range of ~10–100 pM) compared to other miRNAs tested. This finding agrees well with studies reporting relatively high levels of miR-16 in blood serum (Bastus et al., 2011) and over-expression in malignant B-cells of leukemia patients (Cimmino et al., 2005). Our results indicate an over-expression of miR-16 in EL samples of MDS patients. These trends were also observed by the RT-qPCR method (see Table S-3) after total RNA extraction

from the tested samples, although discrepancies in the measured miRNA levels in biological samples by means of RT-qPCR due to RNA extraction can be expected (McAlexander et al., 2013; Turchinovich et al., 2012).

4. Conclusions

We developed a label-free optical biosensor based on SPRi technology for rapid multiplexed detection of miRNAs in real-world erythrocyte lysate (EL) samples with high sensitivity and without the need for RNA extraction. To the best of our knowledge, this is the first work demonstrating the use of an optical label-free biosensor for multiplexed detection of miRNAs in cell lysate. The biosensor utilizes ultra-low fouling carboxy-functional poly(carboxybetaine acrylamide) (pCBAA) coatings and functionalized gold nanoparticles to enhance the sensor response. Using two-step assay, microRNAs were detected in EL in ~45 min at concentrations as low as sub-pM. As the presented SPRi method can detect miRNA directly with no extra EL sample preparation, it may provide more accurate results with respect to methods relying on RNA extraction. We used this biosensor to screen three clinical EL samples for the levels of four miRNAs; we found a higher concentration of miR-16 in EL samples compared to the other three miRNAs tested. These results demonstrate the potential of this SPRi biosensor for the parallelized detection of miRNA in clinical samples. The results indicate that SPR biosensors can ultimately combine the key advantages of current established methods, i.e. the high sensitivity of RT-qPCR and the parallelized detection ability of microarrays.

Acknowledgments

This research was supported by Praemium Academiae of the Academy of Sciences of the Czech Republic, the Czech Science Foundation (contract #P205/12/G118), and the Ministry of Health of the Czech Republic (contract # NT13847-4).

Appendix A. Supplementary material

Supplementary data associated with this article can be found in the online version at http://dx.doi.org/10.1016/j.bios.2015.03.038.

References

Bastus, N.G., Comenge, J., Puntes, V., 2011. Kinetically controlled seeded growth synthesis of citrate-stabilized gold nanoparticles of up to 200 nm: size focusing versus Ostwald ripening. Langmuir 27 (17), 11098–11105.
Benes, V., Castoldi, M., 2010. Expression profiling of microRNA using real-time quantitative PCR, how to use it and what is available. Methods 50 (4), 244–249.
Cheng, Y., Lei, J.P., Chen, Y.L., Ju, H.X., 2014. Highly selective detection of microRNA based on distance-dependent electrochemiluminescence resonance energy transfer between CdTe nanocrystals and Au nanoclusters. Biosens. Bioelectron. 51, 431–436.
Cimmino, A., Calin, G.A., Fabbri, M., Iorio, M.V., Ferracin, M., Shimizu, M., Wojcik, S. E., Aqeilan, R.I., Zupo, S., Dono, M., Rassenti, L., Alder, H., Volinia, S., Liu, C.G., Kipps, T.J., Negrini, M., Croce, C.M., 2005. miR-15 and miR-16 induce apoptosis by targeting BCL2. Proc. Natl. Acad. Sci. USA 102 (39), 13944–13949.
Dong, H.F., Hao, K.H., Tian, Y.P., Jin, S., Lu, H.T., Zhou, S.F., Zhang, X.J., 2014. Label-free and ultrasensitive microRNA detection based on novel molecular beacon binding readout and target recycling amplification. Biosens. Bioelectron. 53, 377–383.
Dong, H.F., Jin, S., Ju, H.X., Hao, K.H., Xu, L.P., Lu, H.T., Zhang, X.J., 2012. Trace and label-free microRNA detection using oligonucleotide encapsulated silver nanoclusters as probes. Anal. Chem. 84 (20), 8670–8674.
Engels, B.M., Hutvagner, G., 2006. Principles and effects of microRNA-mediated post-transcriptional gene regulation. Oncogene 25 (46), 6163–6169.
Erdogan, B., Facey, C., Qualtieri, J., Tedesco, J., Rinker, E., Isett, R.B., Tobias, J., Baldwin, D.A., Thompson, J.E., Carroll, M., Kim, A.S., 2011. Diagnostic microRNAs in myelodysplastic syndrome. Exp. Hematol. 39 (9), 915–926, e912.
Farh, K.K., Grimson, A., Jan, C., Lewis, B.P., Johnston, W.K., Lim, L.P., Burge, C.B., Bartel, D.P., 2005. The widespread impact of mammalian microRNAs on mRNA repression and evolution. Science 310 (5755), 1817–1821.
Felli, N., Fontana, L., Pelosi, E., Botta, R., Bonci, D., Facchiano, F., Liuzzi, F., Lulli, V., Morsilli, O., Santoro, S., Valtieri, M., Calin, G.A., Liu, C.G., Sorrentino, A., Croce, C. M., Peschle, C., 2005. MicroRNAs 221 and 222 inhibit normal erythropoiesis and erythroleukemic cell growth via kit receptor down-modulation. Proc. Natl. Acad. Sci. USA 102 (50), 18081–18086.
Gao, X.F., Xu, H., Baloda, M., Gurung, A.S., Xu, L.P., Wang, T., Zhang, X.J., Liu, G.D., 2014. Visual detection of microRNA with lateral flow nucleic acid biosensor. Biosens. Bioelectron. 54, 578–584.
Gao, Z.Q., Deng, H.M., Shen, W., Ren, Y.Q., 2013. A label-free biosensor for electrochemical detection of femtomolar microRNAs. Anal. Chem. 85 (3), 1624–1630.
Ge, Z.L., Lin, M.H., Wang, P., Pei, H., Yan, J., Sho, J.Y., Huang, Q., He, D.N., Fan, C.H., Zuo, X.L., 2014. Hybridization chain reaction amplification of microRNA detection with a tetrahedral dna nanostructure-based electrochemical biosensor. Anal. Chem. 86 (4), 2124–2130.
Georgantas 3rd, R.W., Hildreth, R., Morisot, S., Alder, J., Liu, C.G., Heimfeld, S., Calin, G.A., Croce, C.M., Civin, C.I., 2007. CD34+ hematopoietic stem-progenitor cell microRNA expression and function: a circuit diagram of differentiation control. Proc. Natl. Acad. Sci. USA 104 (8), 2750–2755.
Guo, S., Yang, F., Zhang, Y.L., Ning, Y., Yao, Q.F., Zhang, G.J., 2014. Amplified fluorescence sensing of miRNA by combination of graphene oxide with duplex-specific nuclease. Anal. Methods 6 (11), 3598–3603.
He, L., Hannon, G.J., 2004. Micrornas: small RNAs with a big role in gene regulation. Nat. Rev. Genet. 5 (7), 522–531.
Homola, J., 2006. Surface Plasmon Resonance Based Sensors. Springer-Verlag.
Homola, J., 2008. Surface plasmon resonance sensors for detection of chemical and biological species. Chem. Rev. 108 (2), 462–493.
Homola, J., Dostalek, J., Chen, S.F., Rasooly, A., Jiang, S.Y., Yee, S.S., 2002. Spectral surface plasmon resonance biosensor for detection of staphylococcal enterotoxin B in milk. Int. J. Food Microbiol. 75 (1–2), 61–69.
Ikeda, S., Kong, S.W., Lu, J., Bisping, E., Zhang, H., Allen, P.D., Golub, T.R., Pieske, B., Pu, W.T., 2007. Altered microRNA expression in human heart disease. Physiol. Genomics 31 (3), 367–373.
Iorio, M.V., Ferracin, M., Liu, C.G., Veronese, A., Spizzo, R., Sabbioni, S., Magri, E., Pedriali, M., Fabbri, M., Campiglio, M., Menard, S., Palazzo, J.P., Rosenberg, A., Musiani, P., Volinia, S., Nenci, I., Calin, G.A., Querzoli, P., Negrini, M., Croce, C.M., 2005. MicroRNA gene expression deregulation in human breast cancer. Cancer Res. 65 (16), 7065–7070.
Kilic, T., Topkaya, S.N., Ariksoysal, D.O., Ozsoz, M., Ballar, P., Erac, Y., Gozen, O., 2012. Electrochemical based detection of microRNA, mir21 in breast cancer cells. Biosens. Bioelectron. 38 (1), 195–201.
Kuchar, M., Vankova, L., Petrokova, H., Cerny, J., Osicka, R., Pelak, O., Sipova, H., Schneider, B., Homola, J., Sebo, P., Kalina, T., Maly, P., 2014. Human interleukin-23 receptor antagonists derived from an albumin-binding domain scaffold inhibit IL-23-dependent ex vivo expansion of IL-17-producing T-cells. Proteins—Struct. Funct. Bioinform. 82 (6), 975–989.
Lagos-Quintana, M., Rauhut, R., Yalcin, A., Meyer, J., Lendeckel, W., Tuschl, T., 2002. Identification of tissue-specific microRNAs from mouse. Curr. Biol. 12 (9), 735–739.
Lahiri, J., Isaacs, L., Tien, J., Whitesides, G.M., 1999. A strategy for the generation of surfaces presenting ligands for studies of binding based on an active ester as a common reactive intermediate: a surface plasmon resonance study. Anal. Chem. 71 (4), 777–790.
Li, F.Y., Peng, J., Wang, J.J., Tang, H., Tan, L., Xie, Q.J., Yao, S.Z., 2014. Carbon nanotube-based label-free electrochemical biosensor for sensitive detection of miRNA-24. Biosens. Bioelectron. 54, 158–164.
Liu, C.G., Calin, G.A., Meloon, B., Gamliel, N., Sevignani, C., Ferracin, M., Dumitru, C. D., Shimizu, M., Zupo, S., Dono, M., Alder, H., Bullrich, F., Negrini, M., Croce, C.M., 2004. An oligonucleotide microchip for genome-wide microRNA profiling in human and mouse tissues. Proc. Natl. Acad. Sci. USA 101 (26), 9740–9744.
Liu, T., Chen, X., Hong, C.Y., Xu, X.P., Yang, H.H., 2014. Label-free and ultrasensitive electrochemiluminescence detection of microRNA based on long-range self-assembled DNA nanostructures. Microchim. Acta 181 (7–8), 731–736.
Lu, J., Getz, G., Miska, E.A., Alvarez-Saavedra, E., Lamb, J., Peck, D., Sweet-Cordero, A., Ebet, B.L., Mak, R.H., Ferrando, A.A., Downing, J.R., Jacks, T., Horvitz, H.R., Golub, T.R., 2005. MicroRNA expression profiles classify human cancers. Nature 435 (7043), 834–838.
McAlexander, M.A., Phillips, M.J., Witwer, K.W., 2013. Comparison of methods for miRNA extraction from plasma and quantitative recovery of rna from cerebrospinal fluid. Front. Genet. 4, 83.
Peng, Y.F., Gao, Z.Q., 2011. Amplified detection of microRNA based on ruthenium oxide nanoparticle-initiated deposition of an insulating film. Anal. Chem. 83 (3), 820–827.
Piliarik, M., Bockova, M., Homola, J., 2010. Surface plasmon resonance biosensor for parallelized detection of protein biomarkers in diluted blood plasma. Biosens. Bioelectron. 26 (4), 1656–1661.
Ren, Y.Q., Deng, H.M., Shen, W., Gao, Z.Q., 2013. A highly sensitive and selective electrochemical biosensor for direct detection of micrornas in serum. Anal. Chem. 85 (9), 4784–4789.
Rhyasen, G.W., Starczynowski, D.T., 2012. Deregulation of microRNAs in myelodysplastic syndrome. Leukemia 26 (1), 13–22.
Rodriguez-Emmenegger, C., Houska, M., Alles, A.B., Brynda, E., 2012. Surfaces

resistant to fouling from biological fluids: towards bioactive surfaces for real applications. Macromol. Biosci. 12 (10), 1413–1422.
Ryoo, S.R., Lee, J., Yeo, J., Na, H.K., Kim, Y.K., Jang, H., Lee, J.H., Han, S.W., Lee, Y., Kim, V.N., Min, D.H., 2013. Quantitative and multiplexed microRNA sensing in living cells based on peptide nucleic acid and nano graphene oxide (PANGO). ACS Nano 7 (7), 5882–5891.
Sipova, H., Homola, J., 2013. Surface plasmon resonance sensing of nucleic acids: a review. Anal. Chim. Acta 773, 9–23.
Sipova, H., Zhang, S.L., Dudley, A.M., Galas, D., Wang, K., Homola, J., 2010. Surface plasmon resonance biosensor for rapid label-free detection of microribonucleic acid at subfemtomole level. Anal. Chem. 82 (24), 10110–10115.
Springer, T., Ermini, M.L., Spackova, B., Jablonku, J., Homola, J., 2014. Enhancing sensitivity of SPR biosensors by functionalized gold nanoparticles-size matters. Anal. Chem.
Springer, T., Piliarik, M., Homola, J., 2010. Surface plasmon resonance sensor with dispersionless microfluidics for direct detection of nucleic acids at the low femtomole level. Sens. Actuators B—Chem. 145 (1), 588–591.
Thomson, J.M., Parker, J., Perou, C.M., Hammond, S.M., 2004. A custom microarray platform for analysis of microRNA gene expression. Nat. Methods 1 (1), 47–53.
Turchinovich, A., Weiz, L., Burwinkel, B., 2012. Extracellular miRNAs: the mystery of their origin and function. Trends Biochem. Sci. 37 (11), 460–465.
Vaisocherova, H., Mrkvova, K., Piliarik, M., Jinoch, P., Steinbachova, M., Homola, J., 2007. Surface plasmon resonance biosensor for direct detection of antibody against Epstein-Barr virus. Biosens. Bioelectron. 22 (6), 1020–1026.
Vaisocherova, H., Sevcu, V., Adam, P., Spackova, B., Hegnerova, K., Pereira, A.D., Rodriguez-Emmenegger, C., Riedel, T., Houska, M., Brynda, E., Homola, J., 2014. Functionalized ultra-low fouling carboxy- and hydroxy-functional surface platforms: functionalization capacity, biorecognition capability and resistance to fouling from undiluted biological media. Biosens. Bioelectron. 51, 150–157.
Vaisocherova, H., Yang, W., Zhang, Z., Cao, Z., Cheng, G., Piliarik, M., Homola, J., Jiang, S., 2008. Ultralow fouling and functionalizable surface chemistry based on a zwitterionic polymer enabling sensitive and specific protein detection in undiluted blood plasma. Anal. chem. 80 (20), 7894–7901.
Valoczi, A., Hornyik, C., Varga, N., Burgyan, J., Kauppinen, S., Havelda, Z., 2004. Sensitive and specific detection of microRNAs by northern blot analysis using LNA-modified oligonucleotide probes. Nucleic Acids Res. 32 (22).
Wang, K., Zhang, S.L., Marzolf, B., Troisch, P., Brightman, A., Hu, Z.Y., Hood, L.E., Galas, D.J., 2009. Circulating microRNAs, potential biomarkers for drug-induced liver injury. Proc. Natl. Acad. Sci. USA 106 (11), 4402–4407.
Wark, A.W., Lee, H.J., Corn, R.M., 2008. Multiplexed detection methods for profiling microRNA expression in biological samples. Angew. Chem.—Int. Ed. 47 (4), 644–652.
Wen, Y.L., Liu, G., Pei, H., Li, L.Y., Xu, Q., Liang, W., Li, Y., Xu, L., Ren, S.Z., Fan, C.H., 2013. DNA nanostructure-based ultrasensitive electrochemical microRNA biosensor. Methods 64 (3), 276–282.
Yin, H.S., Wang, M., Zhou, Y.L., Zhang, X.Y., Sun, B., Wang, G.H., Ai, S.Y., 2014. Photoelectrochemical biosensing platform for microRNA detection based on in situ producing electron donor from apoferritin-encapsulated ascorbic acid. Biosens. Bioelectron. 53, 175–181.
Yin, H.S., Zhou, Y.L., Zhang, H.X., Meng, X.M., Ai, S.Y., 2012. Electrochemical determination of microRNA-21 based on graphene, LNA integrated molecular beacon, AuNPs and biotin multifunctional bio bar codes and enzymatic assay system. Biosens. Bioelectron. 33 (1), 247–253.
Zhang, D.C., Yan, Y.R., Cheng, W., Zhang, W., Li, Y.H., Ju, H.X., Ding, S.J., 2013. Streptavidin-enhanced surface plasmon resonance biosensor for highly sensitive and specific detection of microRNA. Microchim. Acta 180 (5–6), 397–403.
Zhu, W.Y., Su, X.P., Gao, X.Y., Dai, Z., Zou, X.Y., 2014. A label-free and PCR-free electrochemical assay for multiplexed microRNA profiles by ligase chain reaction coupling with quantum dots barcodes. Biosens. Bioelectron. 53, 414–419.